Biomaterials 300 (2023) 122204

Contents lists available at ScienceDirect

Biomaterials

journal homepage: www.elsevier.com/locate/biomaterials

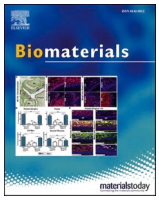

Orally delivered 2D covalent organic frameworks releasing kynurenine generate anti-inflammatory T cell responses in collagen induced arthritis mouse model

Madhan Mohan Chandra Sekhar Jaggarapu [a], Abhirami Thumsi [b], Richard Nile [a], Brian D Ridenour [a], Taravat Khodaei [a], Abhirami P Suresh [b], Arezoo Esrafili [a], Kailong Jin [a,c], Abhinav P Acharya [a,b,d,e,f,g,*]

[a] Chemical Engineering, School for the Engineering of Matter, Transport, and Energy, Arizona State University, Tempe, AZ, 85281, USA
[b] Biological Design, School for the Engineering of Matter, Transport, and Energy, Arizona State University, Tempe, AZ, 85281, USA
[c] Biodesign Center for Sustainable Macromolecular Materials and Manufacturing, Arizona State University, Tempe, AZ, 85281, USA
[d] Biomedical Engineering, School of Biological and Health Systems Engineering, Arizona State University, Tempe, AZ, 85281, USA
[e] Materials Science and Engineering, School for the Engineering of Matter, Transport, and Energy, Arizona State University, Tempe, AZ, 85281, USA
[f] Biodesign Center for Immunotherapy, Vaccines and Virotherapy, Arizona State University, Tempe, AZ, 85281, USA
[g] Biodesign Center for Biodesign Center for Biomaterials Innovation and Translation, Arizona State University, Tempe, AZ, 85281, USA

ARTICLE INFO

Keywords:
Covalent organic framework
Rheumatoid arthritis
Kynurenine
Metabolites
Drug delivery

ABSTRACT

Covalent organic framework (COF) crystalline biomaterials have great potential for drug delivery since they can load large amounts of small molecules (e.g. metabolites) and release them in a controlled manner, as compared to their amorphous counterparts. Herein, we screened different metabolites for their ability to modulate T cell responses *in vitro* and identified Kynurenine (KyH) as a key metabolite that not only decreases frequency of pro-inflammatory RORgt + T cells but also supports frequency of anti-inflammatory GATA3+ T cells. Moreover, we developed a methodology to generate imine-based TAPB-PDA COF at room temperature and loaded these COFs with KyH. KyH loaded COFs (COF-KyH) were able to then release KyH in a controlled manner for 5 days *in vitro*. Notably, COF-KyH when delivered orally in mice induced with collagen-induced rheumatoid arthritis (CIA) were able to increase frequency of anti-inflammatory GATA3+$CD8^+$ T cells in the lymph nodes and decrease antibody titers in the serum as compared to the controls. Overall, these data demonstrate that COFs can be an excellent drug delivery vehicle for delivering immune modulating small molecule metabolites.

1. Introduction

Covalent Organic Frameworks (COFs) possess highly porous and tunable structures that have allowed them to make a great impact in the field of separations, catalysis, and energy storage [1–4]. These materials also show potential in the field of drug delivery due to their biocompatibility/biodegradability, customizable pore size, and dispersibility in biological media [5]. In particular, imine-linked two-dimensional (2D) COFs are attractive due to their convenient syntheses under ambient conditions, immense structural versatility, and excellent crystallinity and biocompatibility [6]. With proper structural design, these imine-linked 2D COFs could form highly regular cylindrical pores suitable for adsorption of small molecules for biological applications [7].

Different crystalline materials have been researched for drug delivery, including COFs [1,3]. However, delivery of immuno-active small molecule metabolites has not been researched. Interestingly, imine-based COFs are negatively charged associated with them [8,9], and thus can be excellent materials for adsorbing positively charged small molecule metabolites, which are difficult to adsorb and deliver using traditional crystalline or amorphous polymeric matrices [10–12]. In fact, positively charged small molecule metabolites such as Kynurenic acid (KyH), spermine, spermidine among others can directly modulate immune cell responses toward anti-inflammatory state [13–17]. However, it is not understood which metabolites induce both upregulation of anti-inflammatory T cells and down-regulation of pro-inflammatory T

* Corresponding author. 550 GWC 651 E. Tyler Mall Tempe, AZ, USA
E-mail address: abhi.acharya@asu.edu (A. P Acharya).

https://doi.org/10.1016/j.biomaterials.2023.122204
Received 28 December 2022; Received in revised form 29 May 2023; Accepted 9 June 2023
Available online 13 June 2023
0142-9612/© 2023 Elsevier Ltd. All rights reserved.

cells, which is essential for generating an effective anti-inflammatory response [11,12,18]. Thus, there is a need to identify a small molecule metabolite that actively modulates T cell responses. Moreover, since these metabolites are metabolized at a quick rate [19], there is a need for development of biomaterials that can adsorb these metabolites in large amount and release them in a controlled manner.

Herein, an approach to generate imine-linked COFs at room temperature was utilized. Additionally, in this study a set of metabolites known to modulate immune responses were screened and KyH was identified as an important metabolite for their ability to modulate anti- and pro-inflammatory T cells *in vitro*. Moreover, room temperature synthesized COFs were able to adsorb KyH and release them in a controlled manner *in vitro*. To demonstrate the utility of these materials as a proof of concept, a Rheumatoid Arthritis (RA) model was utilized [19], where orally delivered KyH loaded COFs were able to modulate T cell responses in the lymph nodes of these mice. Overall, this study demonstrates the use of room temperature synthesized COFs for delivery of immune system modulating metabolites. To the best of our knowledge, this is the first study to demonstrate that imine-linked COFs can be used to adsorb and deliver negatively charged immunomodulating KyH (Fig. 1). In addition to KyH, this system can now be utilized to deliver different types of charged small molecule metabolites for immunosuppressive application.

2. Materials and methods

2.1. Materials

KyH (TCI), itaconic acid, TAPB, PDA, 1,4-dioxane, mesitylene (Sigma Aldrich), spermine (Ambeed), spermidine, lactic acid (Sigma Aldrich), malic acid, succinic acid, putrescine, fumaric acid, and citric acid (Fisher scientific) were purchased and used without any modification. Solvents, catalysts, and monomers including 1,4-dioxane (99.0%, Sigma Aldrich), mesitylene (99% Acros Organics), tetrahydrofuran (99.5%, Supelco), methanol (99.8%, Oakwood Chemical), glacial acetic acid (99.7%, Fisher Chemical), 1,3,5-tris(4-aminophenyl)benzene (93%, Tokyo Chemical Industry), and terephthalaldehyde (98%, Tokyo Chemical Industry) were used as received without further purification.

2.2. Synthesis of COF

In a typical synthesis of this imine-linked TAPB-PDA COF, TAPB (86.95 mg, 0.230 mmol) and PDA (47.24 mg, 0.345 mmol) monomers were combined in a 20 mL scintillation vial. 9.96 mL of 1,4-dioxane/mesitylene (4:1 v/v) solvent mixture was then added to the vial, and the COF building blocks were dissolved with 60 s of ultrasonication. Subsequently, 4.74 mL of 10.5 M acetic acid catalyst was added to the vial which was sealed and left to react at room temperature (~20 °C) under agitation for 72 h. The solid COF product was isolated by vacuum filtration and rinsed thoroughly with tetrahydrofuran followed by methanol. The COF product wet with methanol was then transferred into paper bags (VWR Grade 413 filter paper folded and stapled) for supercritical CO_2 drying (Leica EM CPD300 using 99 rinse cycles), resulting in fluffy yellow powders (88.70 mg, 77.3% yield). Notably, the TAPB-PDA COF product was not allowed to dry at any point prior to supercritical CO_2 drying to prevent the collapse of its mesoporous structure due to the capillary force induced by conventional solvent drying.

2.3. Characterizations of COF

Fourier-transform infrared (FT-IR) spectra of the as-synthesized COF powders were recorded using a Nicolet iS10 FT-IR spectrometer with 64 scans taken and averaged for each sample. Powder X-ray diffraction (PXRD) measurements were performed on a powder X-ray diffractometer (Malvern PANalytical Aeris) equipped with a PIXcel1D detector in a 2θ Bragg Brentano geometry. N_2 adsorption and desorption isotherms at 77 K of the as-synthesized COF powders were collected using a Micromeritics Tristar II unit. Prior to measurement, samples were activated by purging with dry argon at 150 °C for 12 h. Surface area was determined using the Brunauer–Emmett–Teller (BET) method, and pore width distribution was estimated by non-local density functional theory assuming cylindrical pores for the as-synthesized 2D TAPB-PDA COF powders. Scanning electron microscopy (SEM) was performed on a Helios 5 UX dual beam FIB-SEM operating at 20.00 kV. TAPB-PDA COF powders were transferred to carbon tape and coated with a 10 nm gold layer using a Desk II Denton Vacuum Inc. Sputterer for SEM characterization. Dynamic light scattering (DLS) measurements were performed on a Malvern Zetasizer unit. Specifically, the as-synthesized TAPB-PDA COF

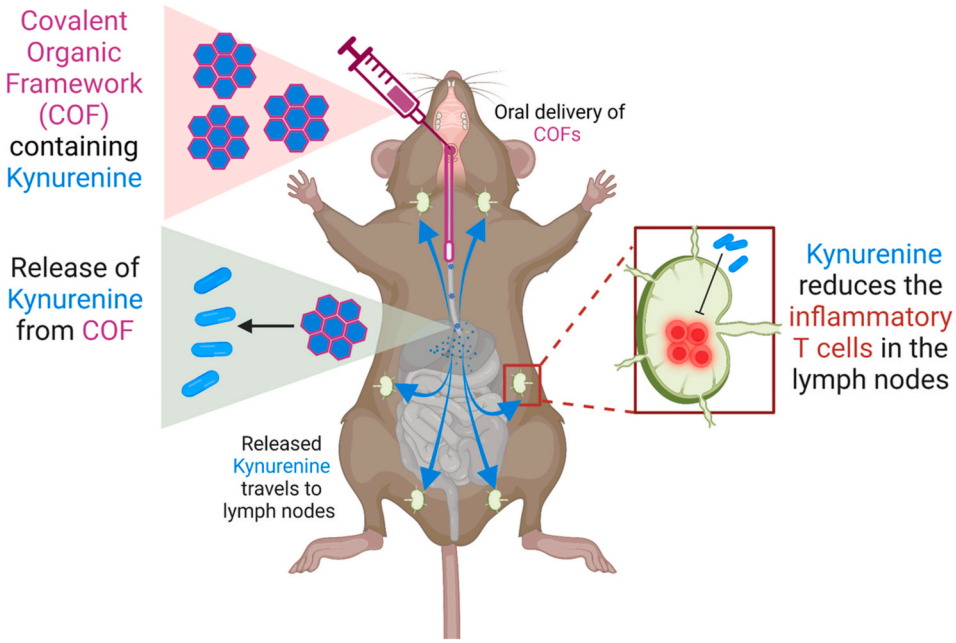

Fig. 1. Schematic of the delivery of Kynurenine (KyH) using COFs for modulating T cell responses.

powders were dispersed in deionized water at 1 mg/mL prior to DLS characterization. Thermal transitions and decompositions of the samples were characterized using TA thermogravimetric analyzer TGA 5500, at 10 °C step increments.

2.4. Degradation study of COFs

The COF powder was suspended at 1 mg/mL in a 10 nM solution of H2O2 in 1X PBS at 37 °C under stirring. Approximately, 3/4 of the liquid volume was replaced with fresh 10 nM H2O2 every other day. The wet powder was collected at 1 day, 3 days, and 7 days. It was then rinsed with deionized water and methanol. The methanol was dried via supercritical CO2 drying. pXRD and FT-IR was performed on these samples as mentioned in the previous paragraph.

2.5. Loading COF with KyH

KyH in 1X PBS were added to 10 mg of COF particles in 1.5 mL centrifuge tubes. This tube was then kept on rotor at room temperature for 24 h. Three different concentrations of KyH at 1 mg/mL, 2 mg/mL, and 3 mg/mL in PBS were incubated with COFs using this procedure. The particles were then washed 3 times in 1X PBS by centrifuging at 2000xGs for 5 min, and then resuspending in 1 mL 1X PBS. The KyH loaded COFs were then freeze dried using lyophilizer and used for further experiments.

2.6. Release kinetics and KyH quantification

The supernatants of COF loaded with KyH were used for the release kinetics study. KyH was dissolved in PBS at a concentration of 1 mg/mL. To this mixture, 10 mg of COF was added and kept on rotor at room temperature for 24 h. After that time, samples were washed with PBS by centrifuging at 2000xGs for 5 min at kept on a rotisserie at 37 °C. At regular intervals of times COF particles were centrifuged at 2000xGs for 5 min and 0.8 mL of supernatant was replaced with fresh 1X PBS. The quantity of KyH from supernatants was determined by using high-performance liquid chromatograph (HPLC, Agilent Technologies, Santa Clara, CA). For the HPLC quantification of KyH, DI water was used as the mobile phase and C18 column as stationary phase. A 50 μL of injection volume, 1.2 mL/min as flow rate was utilized in a Hi-Plex H, 7.7 × 300 mm, 8 μm column (KyH Wavelength = 190 nm).

To determine KyH levels in serum of mice, mice were orally gavaged with COF, KyH or COF-KyH and returned to their cages. After 24 h, mice were euthanized, and serum was isolated. Next, equal volume of methanol was added to the serum in a centrifuge tube, and vortexed vigorously. The tube was then centrifuged at 10,000 xGs for 5 min to remove proteins. The methanol fraction thus obtained was then utilized to determine levels of HPLC and were reported as Absorbance (arbitrary units). The absorbance values were subtracted from samples of COF to obtain absorbance for KyH and COF-KyH.

2.7. CIA induction and treatment

All animal experiments were performed according to the protocol #22–1904R approved by the Animal Care and Use of Experimental Animals (IACUC) at Arizona State University and purchased from Jackson Laboratories. Male DBA/1j and C57BL6/j mice were used for all the studies. Mice were placed in a restrainer and injected subcutaneously one-third of the way down the tail with a complete Freund's adjuvant (CFA) + bovine collagen type II (bc2) emulsion on day 0. Mice were then randomly divided into four groups on day 0 and treated orally with the following: PBS, COF, KyH, and COF-KyH. Mice without induction of CIA were used as control. For the treatment COF-KyH (having 27.8 μg/mouse of KyH) and COF at the dosage of 20 mg/kg were administered in 100 μL of sterile PBS orally. For the KyH treatment group, we used KyH dissolved in 100 μL of sterile PBS equivalent to KyH present in the COF-KyH treatment group. A 100 μL of sterile PBS was orally gavaged for the PBS treatment group and no CIA group. The treatment was given every two days from day 0 till day 18. The mice were euthanized on day 21 and flow analysis of lymphocytes was done on processed lymph nodes.

2.8. Statistical analysis

Statistics were performed using GraphPad Prism. Data were analyzed using a One-way ANOVA followed by Fisher's FSD test, or using Students' ttest, as indicated in figure legends. P values are also detailed in the figure legends.

3. Results and discussion

3.1. Synthesis of COFs

Imine-linked COF was synthesized at room temperature via acetic acid-catalyzed condensation reactions between trifunctional amine (i.e., 1,3,5-tris(4-aminophenyl) benzene; TAPB) and difunctional aldehyde (i.e., Terephthaldehyde; PDA) building blocks (Fig. 2) dissolved in a 1,4-dioxane/mesitylene (4:1 v/v) solvent mixture. After reacting at room temperature for 72 h, the solid COF product was isolated, rinsed thoroughly with tetrahydrofuran and methanol, and dried using supercritical CO_2, resulting in fluffy yellow powders.

As shown in Fig. 2, TAPB-PDA COF can be synthesized via solvothermal reactions between TAPB and PDA monomers which initially lead to imine-linked 2D sheets. As with typical 2D COFs, these sheets rapidly undergo π-π stacking to form crystallites, which eventually undergo random aggregation and precipitate out of solution as powders. TAPB-PDA COF crystallites typically exhibit AA stacking of nanosheets to produce mesoporous hexagonal pores of ~3.3 nm in diameter [6]. Notably, the reaction between TAPB and PDA monomers dissolved in 1, 4-dioxane:mesitylene (4:1 v/v) catalyzed by acetic acid occurs rapidly at room temperature, forming precipitates in seconds. Due to the reversible nature of the imine linkages, the product undergoes a gradual transformation from an initially *amorphous* kinetic product to a thermodynamically favored *crystalline* material over a reaction time of 72 h under the conditions used in this study [7].

The Fourier-transform infrared (FT-IR) spectrum in Fig. 3a confirmed the successful synthesis of TAPB-PDA COF by tracking the disappearance of free aldehyde peak (~1685 cm^{-1}) and appearance of a new peak (~1700 cm^{-1}) corresponding to the C═N stretching of the newly formed imine bonds, in agreement with previous literature [5–7]. According to the powder X-ray diffraction (PXRD) spectrum in Fig. 3b, the as-synthesized TAPB-PDA COF powders developed characteristic diffraction peaks consistent with the expected highly crystalline sheet-like structures in an AA-stacking mode [6]. In support of the PXRD characterization, N_2 adsorption porosimetry (Fig. 3c) reported a type IV isotherm typical of mesoporous materials and a pore size distribution centered at ~3.1 nm (Fig. 3d). Moreover, N_2 adsorption porosimetry of the as-synthesized TAPB-PDA COF powder reported a high surface area of ~1600 $m^2\ g^{-1}$, consistent with its highly crystalline nature based on PXRD. Furthermore, scanning electron microscopy (SEM) images in Fig. 3e revealed that the as-synthesized bulk TAPB-PDA COF powders were comprised of randomly aggregated nanoparticles of ~200 nm in size. The particle size distribution obtained from dynamic light scattering (DLS) in Fig. 3f suggests that when the powder is suspended in deionized water these COF nanoparticles aggregate into clusters of ~1 μm in size, which could further group into super-clusters of ~5 μm in size. Moreover, the zeta potential of the COF particles using zetasizer was determined to be −41.78 ± 1.966 mV in phosphate buffered saline (PBS) at pH 7.4. To study stability of these specific COFs in physiological conditions, they were incubated in 10 nM hydrogen peroxide solution in 1X PBS for 7 days. There were negligible changes in the crystallinity (XRD) and composition (FTIR) of the samples regardless of exposure

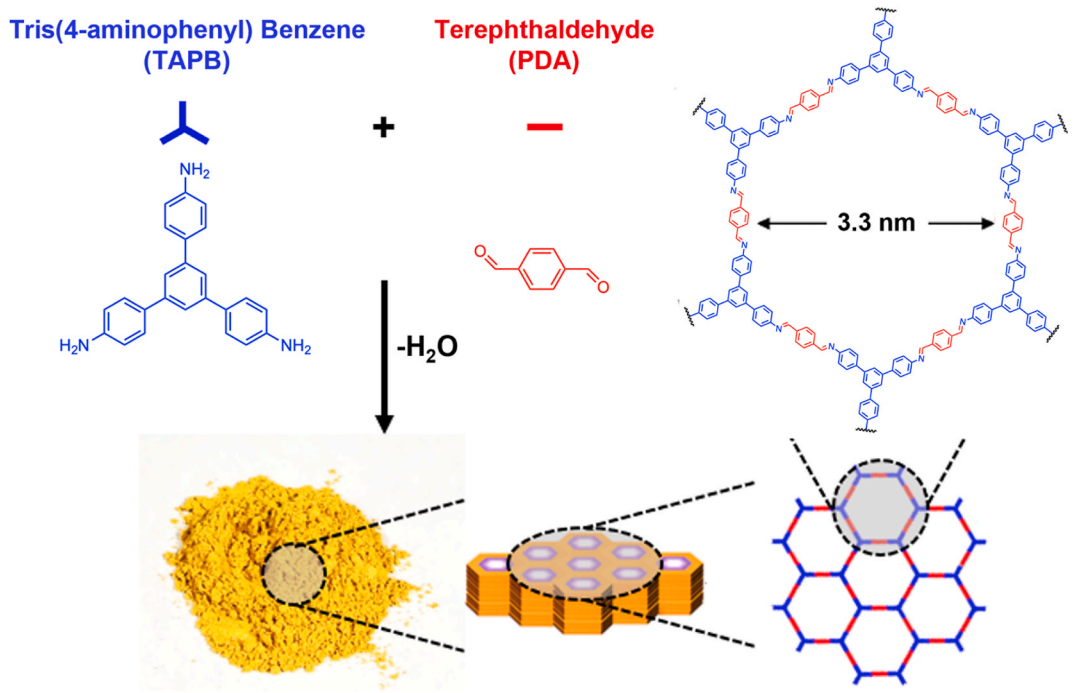

Fig. 2. Reaction scheme for room-temperature solvothermal synthesis of imine-linked TAPB-PDA COF powder, along with illustration of its crystallite structure consisting of stacked 2D sheets (Synthesis adapted from Ref. [5]).

time to hydrogen peroxide in 1X PBS for 7 days, which also was confirmed from previous study [5] for this specific type of COF (Fig. 3g).

3.2. KyH is a promoter of anti-inflammatory T cell phenotype

After generating and synthesizing room temperature COFs, we wanted to test if immuno-active metabolites can be loaded and delivered using this system. In order to test this, first we wanted to choose an appropriate metabolite that would modulate T cell phenotype toward an immunosuppressive nature. Notably, an inflammatory nature of a T cell can be characterized by the transcription factor that it expresses. For example, transcription factor of Tbet and RORgt are associated with expression of pro-inflammatory cytokines IFNg and IL-17 [20,21], respectively; whereas transcription factor of GATA3 and Foxp3 are associated with expression of anti-inflammatory cytokines IL-4 and IL-10 [22,23]. Thus, if a metabolite were to induce an effective anti-inflammatory response, then the frequency of T cells expressive RORgt or Tbet should decrease, while the frequency of T cells expressive GATA3 or Foxp3 Tbet should increase.

To test this hypothesis, we isolated T cells from spleen of C57BL/6j mice [24] and cultured them in the presence of eleven different metabolites namely - alpha ketoglutarate (aKG), citric acid, fumaric acid, Kynurenine, lactic acid, malic acid, putrescine, spermidine, spermine, succinic acid and itaconic acid. These metabolites were chosen because they have found to be elevated in different pro-inflammatory or anti-inflammatory immune responses [12,13,15,25–30]. Flow cytometry was performed on these T cells to identify their phenotype by staining for CD4, Tbet, Foxp3, RORgt, GATA3 and CD44. It was observed that as compared to no treatment control, aKG, citric acid, lactic acid, fumaric acid, succinic acid and itaconic acid increased the frequency of pro-inflammatory Th1 (CD4+Tbet+) cells. Furthermore, metabolites such as kynurenine, putrescine, spermine and spermidine, did significantly change Th1 frequency (Fig. 4a). Notably, kynurenine, putrescine, spermine and spermidine, significantly decreased activated Th1 (CD4+Tbet + $CD44^{+}$) frequency whereas only lactic acid increased the activated Th1 frequency significantly (Fig. 4b). Metabolites such as aKG, fumaric acid, citric acid, lactic acid, malic acid, and succinic acid significantly decreased the total frequency of Th17 (CD4+RORgt+) cell population (Fig. 4c). On the other hand, spermine was the only metabolite that increased Th17 frequency. Kynurenine was not significantly different than no treatment control as far as Th17 frequency was concerned. Importantly, kynurenine, putrescine, spermine, and spermidine significantly decreased frequency of activated Th17 (CD44 + CD4+RORgt+) cells (Fig. 4d). Moreover, aKG, citric acid, fumaric acid, lactic acid, malic acid, and succinic acid led to significantly increased frequency of activated Th17 (CD44 + CD4+RORgt+) cells (Fig. 4d). Notably, in autoimmune diseases such as RA, Th1 and Th17 are the main cell types that attract innate cells such as neutrophils and macrophages to the joint site and lead to tissue destruction [31]. Moreover, activated Th1 and Th17 are the cells responsible for releasing high amounts of cytokines and are the prime target for clinically approved therapeutics, such as methotrexate in the market for reducing inflammation in RA [11].

On the immunosuppressive T cell types, it was observed that aKG, citric acid, fumaric acid, malic acid, and succinic acid led to increased frequency of Th2 (CD4+GATA3+) cells, and spermidine and spermine decreased frequency of Th2 cells as compared to the no treatment control (Fig. 4e). Moreover, kynurenine was not significantly different than the no treatment control. For activated Th2 (CD44 + CD4+GATA3+) cells, lactic acid was the only one that significantly increased their frequency, whereas spermine and spermidine decreased the levels of these cells (Fig. 4f). Interestingly, kynurenine and itaconic acid led to significant increases in regulatory T cell frequency (Tregs - $CD4^{+}$CD25+Foxp3+) as compared to the no treatment control, whereas spermidine and spermine were the only metabolites that decreased Tregs as compared to the no treatment control (Fig. 4g). As far as activated Tregs (CD44 + $CD4^{+}$CD25+Foxp3+) were concerned, citric acid, putrescine, spermine, succinic acid and itaconic acid significantly decreased the frequency as compared to the no treatment control (Fig. 4h). None of the other metabolites significantly modulated activated Treg frequency as compared to the no treatment control.

In terms of cytotoxic T cell (Tc) responses, Tc1 population was not detected in the spermine, and spermidine treated T cells, on the other hand aKG, citric acid, fumaric acid, lactic acid, succinic acid and itaconic

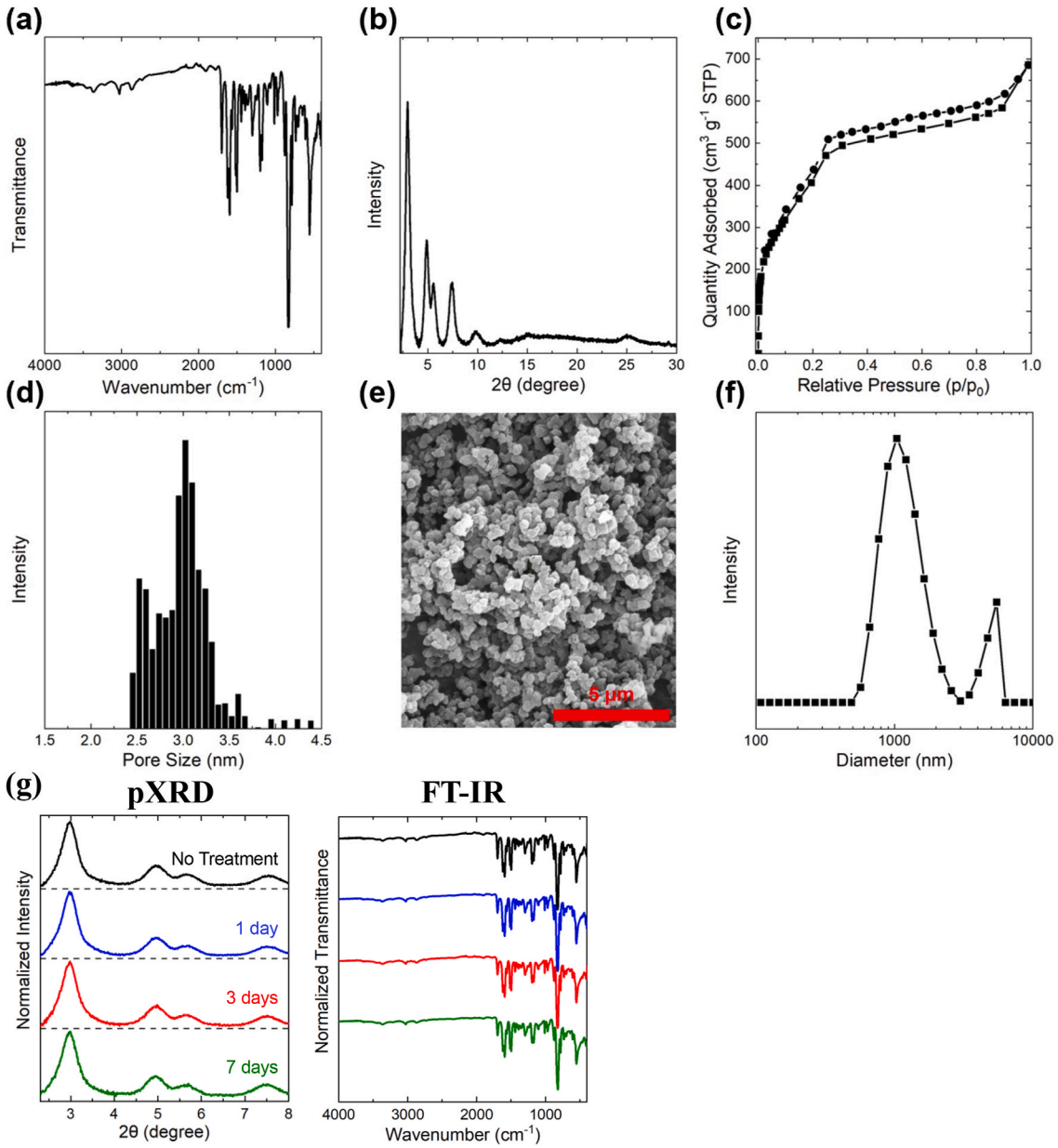

Fig. 3. Characterizations of TAPB-PDA powders: **(a)** Fourier-transform infrared (FT-IR) spectrum; **(b)** Powder X-ray diffraction (PXRD) spectrum; **(c)** Nitrogen adsorption/desorption isotherms at 77 K; **(d)** Non-local density functional theory (NLDFT) pore size distribution; **(e)** Scanning electron microscopy (SEM) image; and **(f)** Dynamic light scattering (DLS) size distribution of the COF powders suspended in deionized water. **(g)** XRD and FT-IR for the stability of COF powders over 7 days in H2O2 in 1X PBS.

acid increased Tc1 frequency (Fig. 5a). Notably, in kynurenine, putrescine, spermine and spermidine, significant decrease in activated Tc1 (CD8+Tbet + $CD44^{+}$) frequency was observed (Fig. 5b). Only itaconic acid, significantly increased the total frequency of Tc17 (CD8+RORgt+) cell population (Fig. 5c). Moreover, activated Tc17 frequency was not detected in any of the conditions after culture of T cells (Fig. 5d). Notably, in autoimmune diseases such as RA, Tc1 are known to accumulate in the joint tissue and lead to inflammation.

On the immunosuppressive T cell types, it was observed that aKG, citric acid, fumaric acid, kynurenine, malic acid, putrescine and succinic acid led to increased frequency of Th2 (CD4+GATA3+) cells, and spermidine and spermine decreased frequency of Tc2 cells as compared to the no treatment control (Fig. 5e). Similar to activated Th2 responses, kynurenine was not significantly different than the no treatment control for Tc2 frequency. For activated Tc2 (CD44 + CD8+GATA3+) cells, lactic acid was the only one that significantly increased their frequency, whereas spermine and spermidine decreased the levels of these cells (Fig. 5f). Interestingly, kynurenine was the only metabolite that led to significant increases in CD8 regulatory T cell frequency (Tregs – $CD8^{+}$CD25+Foxp3+) as compared to the no treatment control, whereas spermidine and spermine were the only metabolites that significantly decreased $CD8^{+}$ Tregs as compared to the no treatment control (Fig. 5g). As far as activated Tregs (CD44 + $CD4^{+}$CD25+Foxp3+) were concerned, citric acid, spermidine, spermine, and itaconic acid significantly decreased the frequency as compared to the no treatment control (Fig. 5h). None of the other metabolites significantly modulated activated $CD8^{+}$ Treg frequency as compared to the no treatment control.

Overall, this data demonstrates that small molecule metabolites by themselves can modulate the levels of pro- and anti-inflammatory cells. More importantly, these results suggest that Kynurenine is able to decrease activated Th17, activated Th1, do not change Th2 cell populations, decrease activated Tc1, increase Tc2, and increase Treg and

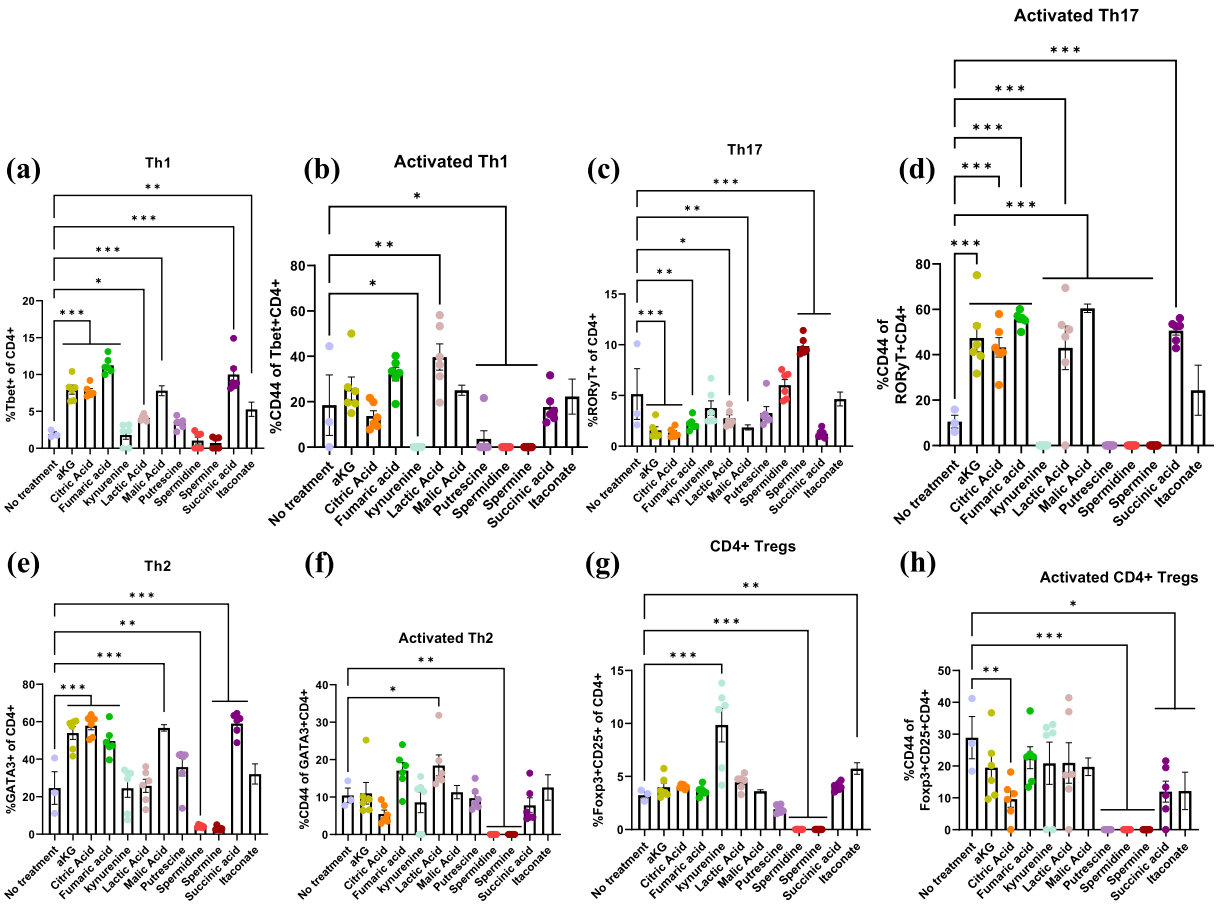

Fig. 4. Metabolites differentially modulate CD4$^+$ T cell phenotype. T helper cells that were modulated by metabolites include, **(a)** T helper type 1 (Th1), **(b)** Activated Th1, **(c)** T helper type 17 (Th17), **(d)** Activated Th17, **(e)** T helper type 2 (Th2), **(f)** Activated Th2, **(g)** Regulatory T cells (Tregs), **(h)** Activated Tregs. N = 6 for metabolites, n = 3 for no treatment, Data represented as Average ± stderror, One-way ANOVA, * - p-values <0.03; ** - p-values <0.002; *** - p-values <0.001.

increase CD8$^+$ Treg levels *in vitro*. Kynurenine is generated by antigen presenting cells such as dendritic cells, by catabolizing tryptophan using indoleamine dioxygenase (IDO) [32]. Tryptophan is essential for the survival and differentiation of Tc1, Th1 and Th17 cells [33,34]. Furthermore, cancer cells also are known to express IDO, which then prevents the functions of these pro-inflammatory cells in the tumor microenvironment [35,36]. Thus, development of a treatment regimen that delivers kynurenine (KyH) can be beneficial in modulating T cell responses in the context of inflammation, such as RA.

3.3. Loading and release of KyH from COFs

From the above results of screening studies with different metabolites, KyH was utilized for further studies as an immunomodulatory metabolite. To test if the KyH was indeed loaded into the COF particles, FT-IR and thermogravimetric analysis (TGA) analysis was performed. Peaks were observed in the FT-IR spectrum of COF-KyH at 3450 cm-1 (primary amine), 3350 cm-1 (aliphatic amine) and 1275 cm-1 (aromatic ketone), which demonstrated the presence of KyH in COFs (Fig. 6a). The encapsulation efficiency of KyH in COF was determined to be 4.6 ± 0.06%, and the loading efficiency was determined to be 32.2 ± 0.4%, which changed with the increasing concentration of KyH incubated with COFs (Fig. 6b). To increase the encapsulation efficiency of KyH in COF, COFs can be chemically modified to be more hydrophilic in order to allow for penetration of KyH in the COFs [3]. Additionally, the poly dispersity index for the particle sizes of the COF particles was determined to be 0.3183. Moreover, the TGA analysis demonstrated approximately 30% weight loss, which was in good agreement with the percentage loading of KyH in COFs (Fig. 6c). As the controlled release is one of the primary characteristics of the delivery system, we choose bulk COF for further studies. To confirm the controlled release pattern of bulk COF at higher amounts of KyH loading, we tested three different loading concentrations of KyH. The release kinetics study results of the KyH from bulk COF-KyH showed a controlled release pattern for 5 days. It was also observed that increasing the loading concentration of KyH, led to increased loading capacity (Fig. 6d). The zeta potential of the COFs generated here was found to be less than - 40 mV in PBS, and thus COFs can co-ordinate with the partial positive charge of the aminobenzene (pKa = 4.6) group on KyH. Moreover, with time, due to inherent instability of the ionic bonds it is expected that the KyH will dissociate from the COFs and get released, which was observed in these experiments (Fig. 6d and e). Since these COFs, are stable in phosphate buffered saline for 5 days, it is not expected that the release of the KyH will occur due to COF degradation. To determine the toxicity of COF-KyH, NIH3T3 cells were cultured for 2 hrs with different concentrations of the particles and alamar blue assays were utilized to determine viability. It was determined that the >80% NIH3T3 cells were alive in the presence of COF-KyH between 0.4 mg/mL to 0.025 mg/mL (Fig. 6f).

3.4. T cell modulation in rheumatoid arthritis due to COF-KyH

After confirming that KyH can be loaded and released from COFs, we next tested if COF-KyH can be used to modulate T cell responses *in vivo*. As a proof of concept, we tested this drug delivery vehicle in a mouse model of RA called collagen induced arthritis model (Fig. 7a). In this model, Arthritis is artificially induced by immunizing the mice against bovine collagen type 2, which then results in inflammation of the joints where collagen is abundant [18]. Importantly, T cells are one of the

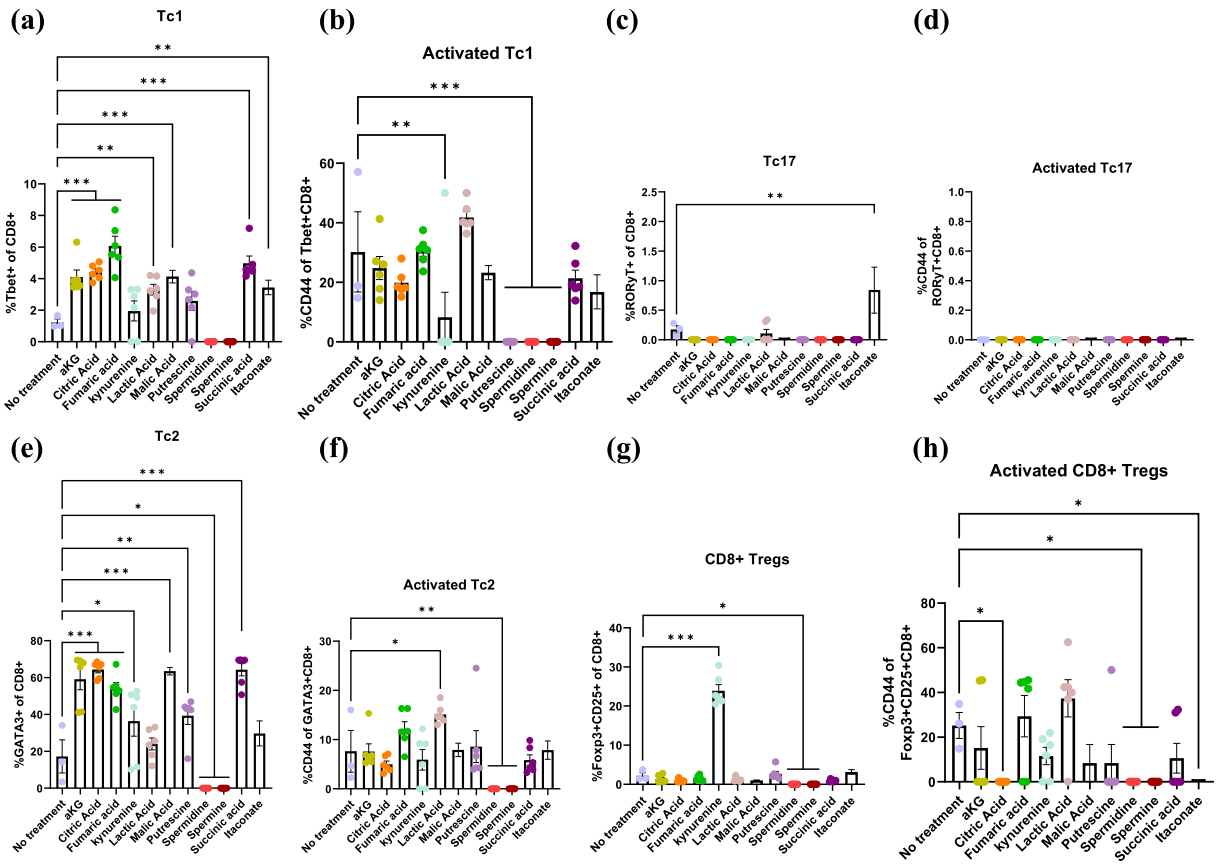

Fig. 5. Metabolites differentially modulate CD8$^+$ T cell phenotype. Cytotoxic T cells that were modulated include **(a)** Cytotoxic T cell type 1 (Tc1), **(b)** Activated Tc1, **(c) Cytotoxic** T cell type 17 (Tc17), **(d)** Activated Tc17, **(e)** Cytotoxic T cell type 2 (Tc2), **(f)** Activated Tc2, **(g)** CD8$^+$ Regulatory T cells (CD8Tregs), **(h)** Activated CD8Tregs. n = 5–6 for all metabolites, n = 3 for no treatment, Data represented as Average ± std error, One-way ANOVA, * - p-values <0.03; ** - p-values <0.002; *** - p-values <0.001.

main immune cell types that propagate this inflammation from the secondary lymphoid organs called lymph nodes. T cells are primed in the lymph nodes to generate pro-inflammatory or anti-inflammatory response [37]. A treatment against RA aims to suppress pro-inflammatory T cells in the lymph node, which can then be observed by analyzing the T cell phenotype in the lymph node using flow cytometry. Therefore, to assess if COF-KyH (highest COF-KyH formulation from loading studies) can generate immunosuppressive CIA was induced in DBA/1j mice on day 0, and COF-KyH were provided to mice via oral gavage. As controls, COF alone, KyH alone or 1X PBS were orally gavaged as well. Moreover, mice without CIA were also used as a control to measure baseline phenotype of T cells. On day 0 after CFA + bc2 injections, we randomly grouped mice into four groups (5 mice per group) and treated them orally with the following conditions PBS, COF, KyH, and COF-KyH. To test if the COF-KyH were indeed able to deliver KyH *in vivo*, mice were orally gavaged with COF-KyH, KyH alone or COF alone, and then sacrificed 24 h later. The serum was analyzed using HPLC, and it was determined that at 24 h time point, there was ~10-fold higher absorbance of KyH in the serum as compared to soluble KyH control (Fig. 7b). These data suggest that the drug delivery vehicle might be able to maintain higher levels of KyH in the blood as compared to soluble delivered KyH.

After treatment of CIA mice for 18 days, mice were euthanized on day 21 to analyze the effect of treatment on T cells. Furthermore, serum was isolated from these mice and antibody titers against collagen type 2 were determined using ELISA. It was determined that the oral delivery of COF-KyH decreased antibody titers in mice against collagen type 2 as compared to the controls (Fig. 7c). This suggests that the COF delivering KyH was able to decrease one of the critical indicators of RA in mice.

To compare the immuno-modulating effect of KyH, COF-KyH with the PBS and COF these mice were euthanized, lymph nodes (inguinal, cervical, and popliteal) were used for flow analysis. The cells were then isolated from these organs and stained for CD4, CD8, CD44, Ki67, CD25, Tbet, Foxp3, GATA3, and RORgT, to identify the T cell phenotype. It was observed that the COF-KyH were able to increase the frequency of Tc2 (GATA3+CD8$^+$) T cells in the inguinal as well as the popliteal lymph nodes, which is the major draining lymph node for the joint paw joint tissue for the mice (Fig. 7d and e). The increase in Tc2 type of cells suggest that the COF-KyH formulation might be able to generate an anti-inflammatory T cell responses *in vivo* in the context of inflammation. Additionally, COF-KyH was able to significantly decrease frequency of Th17 cells in inguinal lymph node as compared to the no treatment control, whereas COF by itself was able to frequency of activated Th17 cells as compared to the no treatment control (Fig. 7f–i). These data suggest that there might gut-joint tissue signaling that might occur, which needs to be further researched.

4. Conclusion

In summary, this study demonstrates that COFs can be utilized to load small molecule metabolites and release these in a controlled manner. Moreover, this study also found that KyH by itself as a metabolite can promote anti-inflammatory T cell responses, and that COFs can release KyH in a controlled manner. Also, these studies show that COF-KyH delivered orally in mice can also modulate T cell function *in vivo* in mice that have RA.

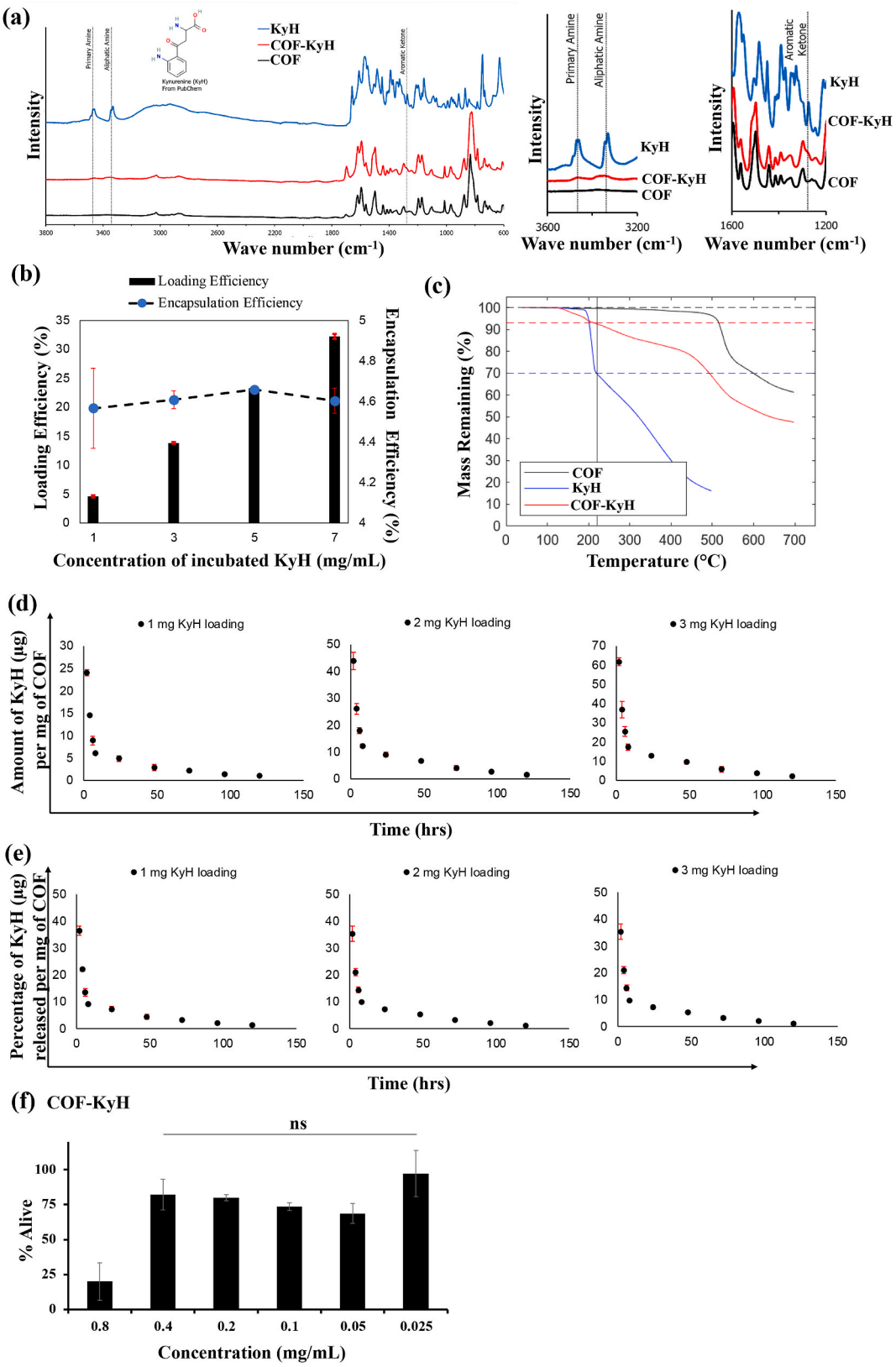

Fig. 6. COFs can load and release Kynurenine (KyH) in a controlled manner. (a) Loading of KyH in COF was confirmed using FTIR (full spectrum on left, with zoomed in images at primary amine, aliphatic amine and aromatic ketone groups on the right). **(b)** Loading efficiency and encapsulation efficiency of KyH in COF at different incubation concentrations. N = 3, Average ± std error. **(c)** Thermogravimetric analysis of KyH in COF demonstrated that approximately 20–30% of KyH was incorporated with COFs. **(d)** Average amount of KyH released from COF versus time N = 3, Data represented as Average ± std error. **(e)** Percentage of KyH released from COF with time. N = 3, Data represented as Average ± std error. **(f)** Viability of NIH3T3 cells N = 3, Data represented as Average ± std error. ns = not significant.

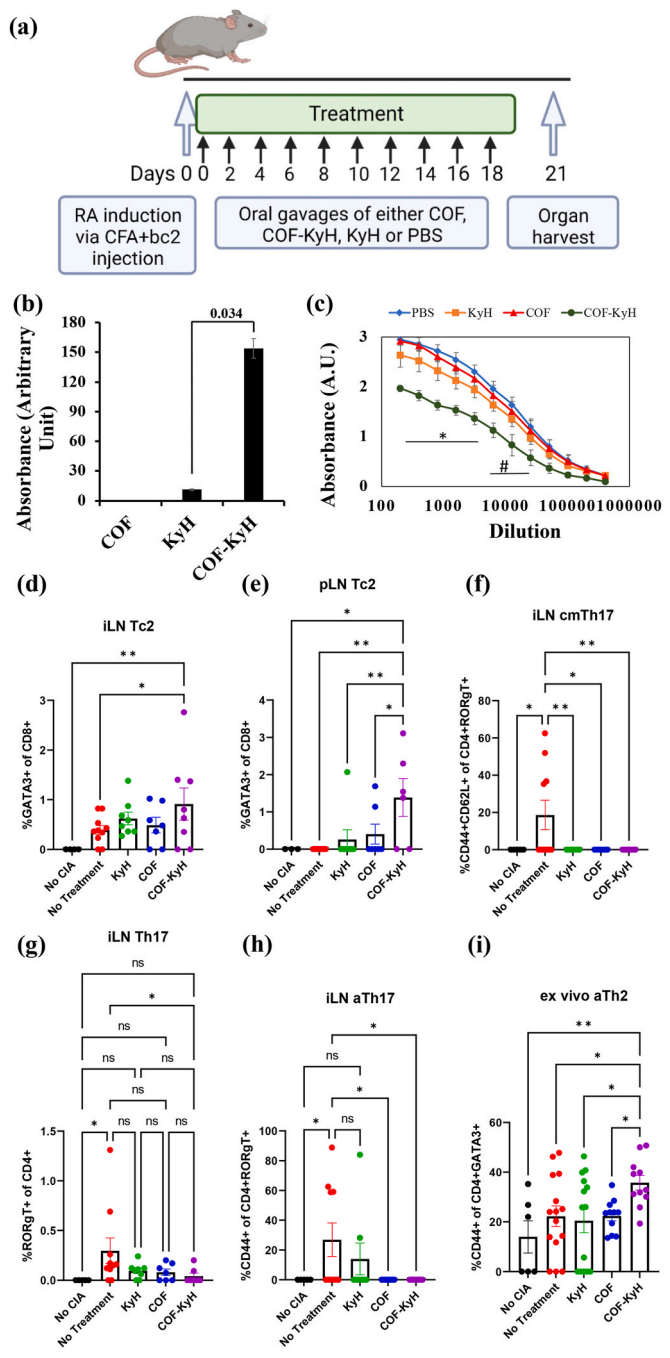

Fig. 7. COFs releasing KyH modulate T cells in Collagen Induced Arthritis (CIA) mouse model. (a) Schematic of the animal model and experiment. **(b)** KyH in the serum of mice orally gavaged with COF-KyH, KyH or COF 24 h after gavage, n = 3, y-axis COF sample subtracted absorbance, Student's t-test, p-value = 0.034. **(c)** Antibody titers are decreased in COF-KyH group as compared to the controls, n = 5 for PBS and KyH, n = 4 for COF and COF-KyH, Student's t-test, * - $p < 0.05$ significant than all conditions, # = $p < 0.05$ significant than PBS. T cell populations modulated by treatment groups include **(d)** Cytotoxic T cell type 2 (Tc2) frequency in inguinal lymph node (iLN), **(e)** Tc2 frequency in popliteal lymph node (pLN), **(f)** Central memory T helper type 17 (cmTh17) in iLN, **(g)** T helper type 17 in iLN, **(h)** Activated Th17 in iLN, and **(i)** Activated T helper type 2 cell frequency that respond to collagen type 2 stimulation. n = 5 for PBS and KyH, n = 4 for COF and COF-KyH, data represented as Average ± std error, one-way ANOVA, * - $p < 0.03$.

Author contributions

MMCSJ performed *in vivo* experiments and wrote the manuscript, AT performed *in vitro* T cell experiments, RN and BDR generated and characterized COFs, TK performed HPLC, APS and AE performed *in vivo* experiments, KJ and APA wrote manuscript.

Declaration of competing interest

The authors declare no competing interest.

Data availability

Data will be made available on request.

Acknowledgements

The authors would like to acknowledge funding sources to APA that supported this work - NIH R01AR078343, and NIH 1R01GM144966-01. The authors would also like to acknowledge the Flow Cytometry Core, the FEI at Erying Materials Center, and the Department of Animal Care and Technologies at Arizona State University. The authors also acknowledge support from the NASA Space Technology Graduate Research Opportunities (NSTGRO) fellowship program (for Richard Nile; Grant 80NSSC21K1274).

References

[1] A. Esrafili, A. Wagner, S. Inamdar, A.P. Acharya, Covalent organic frameworks for biomedical applications, Adv. Healthc. Mater. 10 (2021), 2002090, https://doi.org/10.1002/adhm.202002090.
[2] S. Bhunia, K.A. Deo, A.K. Gaharwar, 2D covalent organic frameworks for biomedical applications, Adv. Funct. Mater. 30 (2020), 2002046, https://doi.org/10.1002/adfm.202002046.
[3] S. Bhunia, M.K. Jaiswal, K.A. Singh, K.A. Deo, A.K. Gaharwar, 2D covalent organic framework direct osteogenic differentiation of stem cells, Adv. Healthc. Mater. 11 (2022), 2101737, https://doi.org/10.1002/adhm.202101737.
[4] M.S. Lohse, T. Bein, Covalent organic frameworks: structures, synthesis, and applications, Adv. Funct. Mater. 28 (2018), 1705553, https://doi.org/10.1002/adfm.201705553.
[5] B.J. Smith, A.C. Overholts, N. Hwang, W.R. Dichtel, Insight into the crystallization of amorphous imine-linked polymer networks to 2D covalent organic frameworks, Chem. Commun. 52 (2016) 3690–3693, https://doi.org/10.1039/C5CC10221A.
[6] D. Zhu, L.B. Alemany, W. Guo, R. Verduzco, Enhancement of crystallinity of imine-linked covalent organic frameworks via aldehyde modulators, Polym. Chem. 11 (2020) 4464–4468, https://doi.org/10.1039/D0PY00776E.
[7] C. Feriante, A.M. Evans, S. Jhulki, I. Castano, M.J. Strauss, S. Barlow, W.R. Dichtel, S.R. Marder, New mechanistic insights into the formation of imine-linked two-dimensional covalent organic frameworks, J. Am. Chem. Soc. 142 (2020) 18637–18644, https://doi.org/10.1021/jacs.0c08390.
[8] F. Benyettou, G. Das, A.R. Nair, T. Prakasam, D.B. Shinde, S.K. Sharma, J. Whelan, Y. Lalatonne, H. Traboulsi, R. Pasricha, O. Abdullah, R. Jagannathan, Z. Lai, L. Motte, F. Gándara, K.C. Sadler, A. Trabolsi, Covalent organic framework embedded with magnetic nanoparticles for MRI and chemo-thermotherapy, J. Am. Chem. Soc. 142 (2020) 18782–18794, https://doi.org/10.1021/jacs.0c05381.
[9] S.A. Ahmed, Q. Liao, Q. Shen, M.M.F. Ashraf Baig, J. Zhou, C. Shi, P. Muhammad, S. Hanif, K. Xi, X. Xia, K. Wang, pH-dependent slipping and exfoliation of layered covalent organic framework, Chem. Eur J. 26 (2020) 12996–13001, https://doi.org/10.1002/chem.202000837.
[10] A.P. Acharya, K.B. Sezginel, H.P. Gideon, A.C. Greene, H.D. Lawson, S. Inamdar, Y. Tang, A.J. Fraser, K.V. Patel, C. Liu, N.L. Rosi, S.Y. Chan, J.L. Flynn, C. E. Wilmer, S.R. Little, In silico identification and synthesis of a multi-drug loaded MOF for treating tuberculosis, J. Contr. Release 352 (2022) 242–255, https://doi.org/10.1016/j.jconrel.2022.10.024.
[11] J.L. Mangal, S. Inamdar, A.P. Suresh, M.M.C.S. Jaggarapu, A. Esrafili, N.D. Ng, A. P. Acharya, Short term, low dose alpha-ketoglutarate based polymeric nanoparticles with methotrexate reverse rheumatoid arthritis symptoms in mice and modulate T helper cell responses, Biomater. Sci. 10 (2022) 6688–6697, https://doi.org/10.1039/d2bm00415a.
[12] J.L. Mangal, S. Inamdar, Y. Yang, S. Dutta, M. Wankhede, X. Shi, H. Gu, M. Green, K. Rege, M. Curtis, A.P. Acharya, Metabolite releasing polymers control dendritic cell function by modulating their energy metabolism, J. Mater. Chem. B 8 (2020) 5195–5203, https://doi.org/10.1039/D0TB00790K.
[13] G.M. Carriche, L. Almeida, P. Stüve, L. Velasquez, A. Dhillon-LaBrooy, U. Roy, M. Lindenberg, T. Strowig, C. Plaza-Sirvent, I. Schmitz, M. Lochner, A.K. Simon, T. Sparwasser, Regulating T-cell differentiation through the polyamine spermidine,

J. Allergy Clin. Immunol. 147 (2021) 335–348.e11, https://doi.org/10.1016/j.jaci.2020.04.037.
[14] R.S. Hesterberg, J.L. Cleveland, P.K. Epling-Burnette, Role of polyamines in immune cell functions, Med. Sci. Basel Switz. 6 (2018) 22, https://doi.org/10.3390/medsci6010022.
[15] E. Proietti, S. Rossini, U. Grohmann, G. Mondanelli, Polyamines and kynurenines at the intersection of immune modulation, Trends Immunol. 41 (2020) 1037–1050, https://doi.org/10.1016/j.it.2020.09.007.
[16] R. Zheng, M. Kong, S. Wang, B. He, X. Xie, Spermine alleviates experimental autoimmune encephalomyelitis via regulating T cell activation and differentiation, Int. Immunopharm. 107 (2022), 108702, https://doi.org/10.1016/j.intimp.2022.108702.
[17] S. Inamdar, T. Tylek, A. Thumsi, A.P. Suresh, M.M.C.S. Jaggarapu, M. Halim, S. Mantri, A. Esrafili, N.D. Ng, E. Schmitzer, K. Lintecum, C. de Ávila, J.D. Fryer, Y. Xu, K.L. Spiller, A.P. Acharya, Biomaterial mediated simultaneous delivery of spermine and alpha ketoglutarate modulate metabolism and innate immune cell phenotype in sepsis mouse models, Biomaterials 293 (2023), 121973, https://doi.org/10.1016/j.biomaterials.2022.121973.
[18] J.L. Mangal, S. Inamdar, T. Le, X. Shi, M. Curtis, H. Gu, A.P. Acharya, Inhibition of glycolysis in the presence of antigen generates suppressive antigen-specific responses and restrains rheumatoid arthritis in mice, Biomaterials 277 (2021), 121079, https://doi.org/10.1016/j.biomaterials.2021.121079.
[19] J.L. Mangal, Neha basu, H.J.J. Wu, A.P. Acharya, Immunometabolism: an emerging target for immunotherapies to treat rheumatoid arthritis, Immunometabolism (2021), https://doi.org/10.20900/immunometab20210032.
[20] I.I. Ivanov, B.S. McKenzie, L. Zhou, C.E. Tadokoro, A. Lepelley, J.J. Lafaille, D. J. Cua, D.R. Littman, The orphan nuclear receptor RORγt directs the differentiation program of proinflammatory IL-17+ T helper cells, Cell 126 (2006) 1121–1133, https://doi.org/10.1016/j.cell.2006.07.035.
[21] S.L. Stone, J.N. Peel, C.D. Scharer, C.A. Risley, D.A. Chisolm, M.D. Schultz, B. Yu, A. Ballesteros-Tato, W. Wojciechowski, B. Mousseau, R.S. Misra, A. Hanidu, H. Jiang, Z. Qi, J.M. Boss, T.D. Randall, S.R. Brodeur, A.W. Goldrath, A. S. Weinmann, A.F. Rosenberg, F.E. Lund, T-Bet transcription factor promotes antibody-secreting cell differentiation by limiting the inflammatory effects of IFN-γ on B cells, Immunity 50 (2019) 1172–1187.e7, https://doi.org/10.1016/j.immuni.2019.04.004.
[22] M. Murai, O. Turovskaya, G. Kim, R. Madan, C.L. Karp, H. Cheroutre, M. Kronenberg, Interleukin 10 acts on regulatory T cells to maintain expression of the transcription factor Foxp3 and suppressive function in mice with colitis, Nat. Immunol. 10 (2009) 1178–1184, https://doi.org/10.1038/ni.1791.
[23] R. Yagi, J. Zhu, W.E. Paul, An updated view on transcription factor GATA3-mediated regulation of Th1 and Th2 cell differentiation, Int. Immunol. 23 (2011) 415–420, https://doi.org/10.1093/intimm/dxr029.
[24] C. Grosjean, J. Quessada, M. Nozais, M. Loosveld, D. Payet-Bornet, C. Mionnet, Isolation and enrichment of mouse splenic T cells for ex vivo and in vivo T cell receptor stimulation assays, STAR Protoc 2 (2021), 100961, https://doi.org/10.1016/j.xpro.2021.100961.
[25] F.A. Boros, L. Vécsei, Immunomodulatory effects of genetic alterations affecting the kynurenine pathway, Front. Immunol. 10 (2019) 2570, https://doi.org/10.3389/fimmu.2019.02570.
[26] M. Carreño, M.F. Pires, S.R. Woodcock, T. Brzoska, S. Ghosh, S.R. Salvatore, F. Chang, N.K.H. Khoo, M. Dunn, N. Connors, S. Yuan, A.C. Straub, S.G. Wendell, G.J. Kato, B.A. Freeman, S.F. Ofori-Acquah, P. Sundd, F.J. Schopfer, D.A. Vitturi, Immunomodulatory actions of a kynurenine-derived endogenous electrophile, Sci. Adv. 8 (2022), eabm9138, https://doi.org/10.1126/sciadv.abm9138.
[27] A. Hooftman, L.A.J. O'Neill, The immunomodulatory potential of the metabolite itaconate, Trends Immunol. 40 (2019) 687–698, https://doi.org/10.1016/j.it.2019.05.007.
[28] G. Kaur, T.B. Shivanandappa, M. Kumar, A.S. Kushwah, Fumaric acid protect the cadmium-induced hepatotoxicity in rats: owing to its antioxidant, anti-inflammatory action and aid in recast the liver function, Naunyn-Schmiedeberg's Arch. Pharmacol. 393 (2020) 1911–1920, https://doi.org/10.1007/s00210-020-01900-7.
[29] C. Nastasi, A. Willerlev-Olsen, K. Dalhoff, S.L. Ford, A.-S.Ø. Gadsbøll, T.B. Buus, M. Gluud, M. Danielsen, T. Litman, C.M. Bonefeld, C. Geisler, N. Ødum, A. Woetmann, Inhibition of succinate dehydrogenase activity impairs human T cell activation and function, Sci. Rep. 11 (2021) 1458, https://doi.org/10.1038/s41598-020-80933-7.
[30] M.J. Palte, A. Wehr, M. Tawa, K. Perkin, R. Leigh-Pemberton, J. Hanna, C. Miller, N. Penner, Improving the gastrointestinal tolerability of fumaric acid esters: early findings on gastrointestinal events with diroximel fumarate in patients with relapsing-remitting multiple sclerosis from the phase 3, open-label EVOLVE-MS-1 study, Adv. Ther. 36 (2019) 3154–3165, https://doi.org/10.1007/s12325-019-01085-3.
[31] K.C. Navegantes, R. de Souza Gomes, P.A.T. Pereira, P.G. Czaikoski, C.H. M. Azevedo, M.C. Monteiro, Immune modulation of some autoimmune diseases: the critical role of macrophages and neutrophils in the innate and adaptive immunity, J. Transl. Med. 15 (2017) 36, https://doi.org/10.1186/s12967-017-1141-8.
[32] E. Wirthgen, A. Hoeflich, A. Rebl, J. Günther, Kynurenic acid: the janus-faced role of an immunomodulatory tryptophan metabolite and its link to pathological conditions, Front. Immunol. 8 (2018) 1957, https://doi.org/10.3389/fimmu.2017.01957.
[33] J. Correale, Immunosuppressive amino-acid catabolizing enzymes in multiple sclerosis, Front. Immunol. 11 (2021), 600428, https://doi.org/10.3389/fimmu.2020.600428.
[34] S.-A. Esmaeili, J. Hajavi, The role of indoleamine 2,3-dioxygenase in allergic disorders, Mol. Biol. Rep. 49 (2022) 3297–3306, https://doi.org/10.1007/s11033-021-07067-5.
[35] A. Pataskar, J. Champagne, R. Nagel, J. Kenski, M. Laos, J. Michaux, H.S. Pak, O. B. Bleijerveld, K. Mordente, J.M. Navarro, N. Blommaert, M.M. Nielsen, D. Lovecchio, E. Stone, G. Georgiou, M.C. de Gooijer, O. van Tellingen, M. Altelaar, R.P. Joosten, A. Perrakis, J. Olweus, M. Bassani-Sternberg, D.S. Peeper, R. Agami, Author Correction: tryptophan depletion results in tryptophan-to-phenylalanine substitutants, Nature 608 (2022) E20, https://doi.org/10.1038/s41586-022-05097-y.
[36] D. Tang, L. Yue, R. Yao, L. Zhou, Y. Yang, L. Lu, W. Gao, P53 prevent tumor invasion and metastasis by down-regulating Ido in lung cancer, Oncotarget 8 (2017) 54548–54557, https://doi.org/10.18632/oncotarget.17408.
[37] H.R. Hampton, T. Chtanova, Lymphatic migration of immune cells, Front. Immunol. 10 (2019) 1168, https://doi.org/10.3389/fimmu.2019.01168.